AIP | Review of Scientific Instruments

Vacuum upgrade and enhanced performances of the double imaging electron/ion coincidence end-station at the vacuum ultraviolet beamline DESIRS

Xiaofeng Tang, Gustavo A. Garcia, Jean-François Gil, and Laurent Nahon

Citation: Review of Scientific Instruments **86**, 123108 (2015); doi: 10.1063/1.4937624
View online: http://dx.doi.org/10.1063/1.4937624
View Table of Contents: http://scitation.aip.org/content/aip/journal/rsi/86/12?ver=pdfcov
Published by the AIP Publishing

Vacuum upgrade and enhanced performances of the double imaging electron/ion coincidence end-station at the vacuum ultraviolet beamline DESIRS

Xiaofeng Tang,[1,2] Gustavo A. Garcia,[1,a)] Jean-François Gil,[1] and Laurent Nahon[1]
[1]*Synchrotron SOLEIL, L'Orme des Merisiers, St. Aubin BP 48, 91192 Gif sur Yvette, France*
[2]*Laboratory of Atmospheric Physico-Chemistry, Anhui Institute of Optics and Fine Mechanics, Chinese Academy of Sciences, Hefei, 230031 Anhui, China*

(Received 29 September 2015; accepted 30 November 2015; published online 21 December 2015)

We report here the recent upgrade of the SAPHIRS permanent photoionization end-station at the DESIRS vacuum ultraviolet beamline of synchrotron SOLEIL, whose performances have been enhanced by installing an additional double-skimmer differential chamber. The smaller molecular beam profile obtained at the interaction region has increased the mass resolution of the double imaging photoelectron photoion coincidence (i^{2}PEPICO) spectrometer, DELICIOUS III, installed in the photoionization chamber of the SAPHIRS endstation, by a factor of two, to M/ΔM ~ 1700 (FWHM). The electron kinetic energy resolution offered by the velocity map imaging (VMI) part of the spectrometer has been improved down to 2.8% (ΔE/E) as we show on the N_2 photoionization case in the double skimmer configuration. As a representative example of the overall state-of-the-art i^{2}PEPICO performances, experimental results of the dissociation of state-selected $O_2^+(B^2\sum_g^-, v^+ = 0\text{-}6)$ molecular ions performed at the fixed photon energy of hν = 21.1 eV are presented. © *2015 AIP Publishing LLC*. [http://dx.doi.org/10.1063/1.4937624]

I. INTRODUCTION

Vacuum ultraviolet (VUV) gas-phase photoionization is a fundamental photon-matter process extensively studied in the laboratory and widely found in natural environments such as planetary ionospheres and the interstellar medium. The methods of photoionization mass spectrometry (PIMS) and photoelectron spectroscopy (PES) as fine probes of molecular photoionization have made considerable progresses in the past decades benefiting from the constant improvement of modern light sources such as laser and synchrotron radiation (SR).[1–5] SR appears as an ideal light source in photoionization experiments because of its high flux, high resolution, wide energy range, and easy tunability in the VUV energy range and polarization control.[6–10] Building on the long established capabilities of PIMS and PES, photoelectron photoion coincidence (PEPICO) spectroscopy offers additional or complementary information as photoionization mass spectra and mass-selected photoelectron spectra can be measured and correlated in coincidence.[11–13] Of particular interest when combined with tunable radiation such as SR, the techniques of threshold photoelectron spectroscopy (TPES) and threshold photoelectron photoion coincidence (TPEPICO) spectroscopy have been frequently utilized in gas-phase photoionization experiments and have provided a lot of valuable information due to the high collection efficiency of threshold electrons associated with a high and constant energy resolution.[14–19]

DELICIOUS III,[19] the double imaging photoelectron photoion coincidence (i^{2}PEPICO) spectrometer consists of a velocity map imaging (VMI) device[20] and a modified Wiley-McLaren time of flight (TOF) momentum imaging analyzer[21] to detect photoelectrons and photoions, respectively, in coincidence. This i^{2}PEPICO spectrometer is installed in one of the permanent end-stations—the molecular beam chamber SAPHIRS[22] of the DESIRS VUV beamline[8] which is located at Synchrotron SOLEIL, the third generation French national synchrotron facility—and has been operated since early 2013. Every year many projects covering a very broad scientific case related to astrophysics, biology, atmospheric chemistry, combustion, nanoscience, and basic atomic and molecular physics are carried out with this very versatile i^{2}PEPICO spectrometer.[23]

In order to meet the DESIRS beamline users' requirements in terms of vacuum (especially for the study of atmospheric room temperature chemistry and the one of nanoparticles) and also improve the performances of the i^{2}PEPICO spectrometer, the molecular beam chamber SAPHIRS,[22] which has been used routinely for more than twenty years in French synchrotron facilities and abroad, has been recently upgraded with the addition of a double-skimmer (DS) differential chamber as described hereafter with the corresponding and additional enhanced performances of the i^{2}PEPICO setup.

II. EXPERIMENTAL SETUP

The detailed configurations of the DESIRS beamline[8] and the i^{2}PEPICO spectrometer DELICIOUS III[19] have already been presented in detail elsewhere, so only a brief description will be outlined here. This part will mainly focus on the change of the SAPHIRS vacuum molecular beam chambers.[22]

A schematic diagram of the SAPHIRS molecular beam chamber with the DELICIOUS III spectrometer inside is

a)Author to whom correspondence should be addressed. Electronic mail: gustavo.garcia@synchrotron-soleil.fr

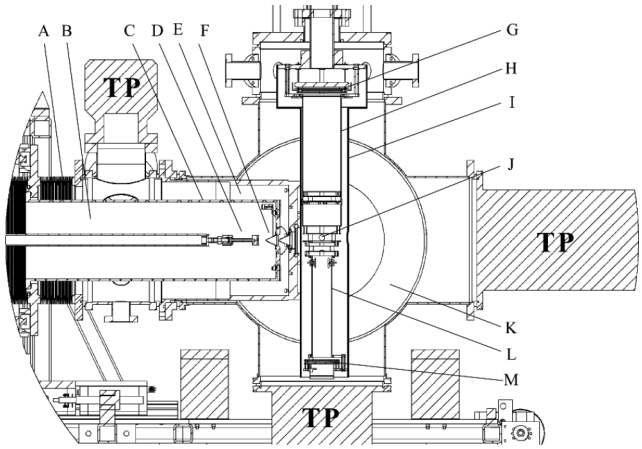

FIG. 1. Overview of the SAPHIRS double-skimmer chambers with the i^{2}PEPICO spectrometer DELICIOUS III inside. To emphasize the change of SAPHIRS, the jet chamber with other two turbo-pumps and the XYZ-manipulator of source have been ignored in the figure. A: XYZ-manipulator for the first skimmer; B: jet chamber; C: movable inner aluminum cylinder; D: nozzle; E: double-skimmer differential chamber; F: skimmers; G: electron delay line detector; H: electron drift tube; I: double layer μ-metal; J: photoionization region; K: ionization chamber; L: ion drift tube; M: ion delay line detector; and TP: turbo-molecular pump.

shown in Figure 1. Other than the previous configuration,[22] an additional new chamber with another skimmer has been installed and now SAPHIRS is composed of three vacuum chambers, a jet or expansion, a DS differential, and an ionization chamber. The jet chamber is evacuated by two turbo-molecular pumps (2000 l/s, Adixen ATP3000M and 1000 l/s Seiko Seiki STPH1000C), the DS chamber by three turbo-molecular pumps (300 l/s, Edwards nEXT300D) and the ionization chamber by two turbo-molecular pumps (1000 l/s, Leybold TurboVac1000). The turbo-molecular pumps of the jet and DS chambers are roughed by the same 120 m^3/h primary pump (Adixen ADP122), and the turbo-molecular pumps of the ionization chamber are backed by a 28 m^3/h primary pump (Adixen ADP28G). The base pressures without gas load in the three chambers are in the low 10^{-8} mbar range.

Depending on the projects,[24–31] various sources such as a simple small aperture nozzle, in-vacuum temperature-controlled ovens coupled to a nozzle for liquid and solid samples, pyrolysis sources or bubblers can be used leading to the formation of a continuous supersonic molecular beam formed by adiabatic expansion. More elaborate sources like an aerosol aerodynamic lens[32] and a fast flow-tube reactor[33] can also be installed and inter-changed quickly in the jet chamber. In all cases the sample source is fixed on a computer-controlled XYZ manipulator and its position can be tuned in vacuum to optimize in real-time the molecular beam. After passing through a first skimmer (Beam Dynamics, Inc.), the molecular beam reaches the DS differential chamber. The position of this first skimmer separating the jet and DS chambers can be optimized under vacuum since its mounting is bolted to a movable inner aluminum cylinder that is connected, via large flexible bellows, to another computer-controlled XYZ manipulator on the outside. Note that, if single skimmer operations were desirable, the first skimmer and its large support plate can be rapidly removed due to the use of a quick-release system based on a threaded mounting. The second skimmer separating the DS chamber from the ionization chamber is located about 15 mm downstream of the first skimmer and mechanically fixed at the center of the chamber. A thin sliding valve behind the second skimmer is installed and used to isolate the ionization chamber when the DS and jet chambers are vented, for instance to refill the sample or exchange sources. Then the molecular beam (MB) arrives at the photoionization region and crosses the synchrotron beam at a right angle in the center of the DELICIOUS III spectrometer.

The typical working pressures in the jet, DS, and ionization chambers are in the 10^{-4}, 10^{-6}, and 10^{-8} mbar ranges, respectively, with the molecular beam on. For certain applications, such as the study of chemical reactivity, the expansion chamber is directly pumped by a 600 m^3/h roots pump (Edwards GX600N) because the typical working pressures in the expansion chamber, a few mTorrs, are not compatible with the turbo-molecular pumps described earlier. This pressure range leads to 10^{-4} and still 10^{-8} mbar inside the DS and spectrometer chamber, respectively.[33] Due to the higher pressures now allowed inside the expansion chamber, larger sample loads can be used by working in the roots regime, and future applications include a larger nanoparticle production by increasing the inlet aperture of aerodynamic lens from the current 160 μm.[32] Another additional and critical advantage of the new DS geometry for the study of the physical and chemical properties of aerosols is the more efficient removal of the gas phase component of the aerosol source.

VUV synchrotron photons emitted from a variable polarization undulator (OPHELIE 2) were monochromatized with a 6.65 m Eagle off-plane normal incidence monochromator and focused onto a spot with ~0.07 mm (V) × 0.2 mm (H) size (for 100 μm slits) in the ionization region. Four gratings (200, 400, 2400, 4300 l/mm) are incorporated in the monochromator to cover the whole energy range of 5–40 eV with a fully adjustable resolution/flux compromise.[8] In the present experiments, only the 200 l/mm grating was used and the polarization of photons was set as linear horizontal. A gas filter located upstream of the beamline was filled with noble gases to efficiently suppress the contributions from higher harmonics of the undulator.

The i^{2}PEPICO spectrometer DELICIOUS III[19] is installed in the ionization chamber of SAPHIRS. The molecular beam, the synchrotron beam and the axis of DELICIOUS III cross each other with a right angle at the ionization region. The electrons and ions produced in the photoionization process were extracted and accelerated vertically in opposite directions by a VMI[20] device and a modified Wiley-McLaren TOF[21] imaging analyzer, respectively. The full 3D ion momentum distribution was acquired from its TOF, measured with respect to the arrival time of the corresponding electron, and its position on the custom-made 40 mm ion position sensitive detector (PSD). Another, larger, PSD detector (80 mm, DLD80, Roentdek) was used to collect electron images on the VMI which can be processed with ion mass- and momentum-selection in the coincidence scheme. An Abel inversion algorithm[34] was used

to treat electron images to get the electron angular distribution and photoelectron spectrum. In addition, combining the electron and ion images in coincidence provides electron and ion kinetic energy correlation diagrams.[26,27]

III. RESULTS AND DISCUSSION

A. Size of molecular beam

One of the main purposes of upgrading the SAPHIRS chambers is to reduce the size of molecular beam in the photoionization region by using a double-skimmer geometry as commonly used in the molecular dynamics community.[35] To show the actual size of the molecular beam, the ion projection image[19,33] of Ar^+ has been acquired at hν = 17 eV in the single-skimmer geometry and is shown in Figure 2(a), exhibiting the classical elongated cigar shape along the photon axis. The molecular beam propagates horizontally from the east to the west in the image and the direction of the synchrotron beam is from the north to the south. Due to the speed of molecular beam, the image is displaced from the detector center. The horizontal dimension of the SR (along MB) is 200 μm FWHM,[8] which, convoluted with the spread due to the translational temperature, leads to the spread along the x-axis seen in Figure 2(a). Ray-tracing numerical simulations using a custom-made code yield, in comparison to Fig. 2(a), a translational temperature close to 40 K, and a beam diameter close to 7 mm.

As seen in the Ar^+ image shown in Fig. 2(b), and its associated SR projection shown in red in Fig. 2(c), recorded under the same experimental conditions as in Fig. 2(a), addition of the double skimmer shortens the North-South length by close to a factor of two, so that the width of the molecular beam is now reduced to 4 mm. The two intensity distributions shown in Fig. 2(d) are integrated along the direction of the molecular beam and thus, as explained above, have the same shape given by the SR horizontal spread. However, the intensity distributions in Figure 2(d) can be divided into two parts, an intense part with a displacement from the center due to the speed of the molecular beam which is attributed to the cold molecular beam, and a much weaker component centered around the zero position due to the room temperature background gas.[33] We can see that the amount of background gas has been noticeably reduced upon the addition of the double-skimmer, indicating that a more collimated molecular beam has been formed. Furthermore, as seen in Fig. 2(d) where the data have been normalized to the experimental count-rate, for a given nozzle-interaction region distance, there is virtually no loss of signal on the supersonic component, and only the thermal part disappears. Ion images recorded at the same fixed nozzle-interaction region distance show that the beam profile is 30% smaller when doubly skimmed, and therefore the effect of the DS chamber on the size of the beam is more positive than merely reducing the solid angle by augmenting this distance. However, the minimum distance from the nozzle to the interaction region is increased with the presence of the DS chamber. Therefore, the maximum signal attainable will be limited because we have observed experimentally that the ionization signal decreases with the square root of this distance.

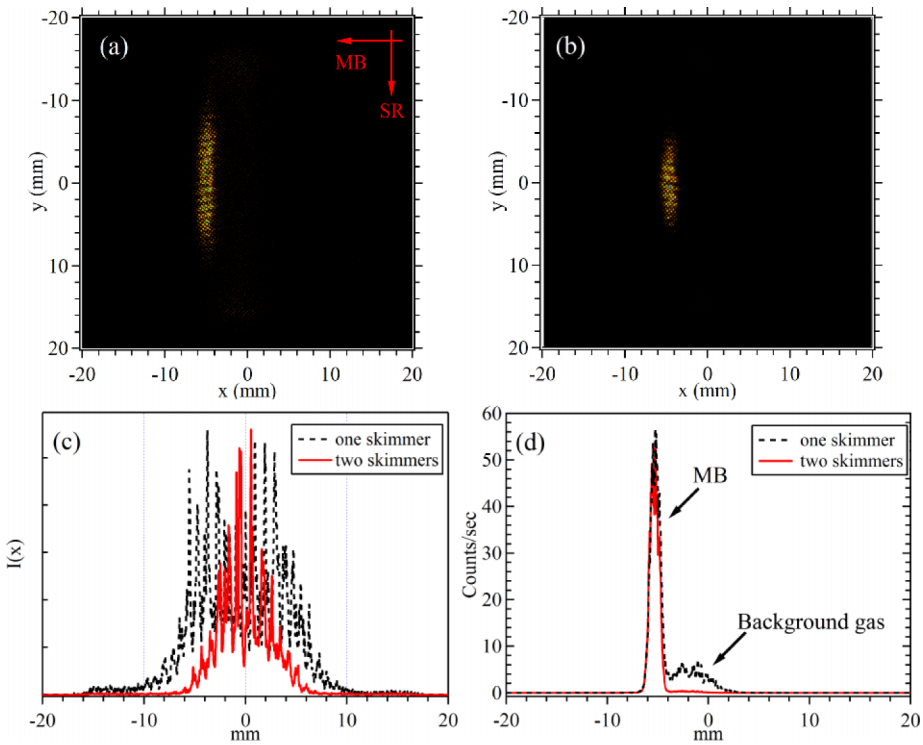

FIG. 2. The ion projection images of Ar^+ recorded at hν = 17 eV with (a) one skimmer and (b) two skimmers. The image projection integrated along the (c) x-axis and (d) y-axis directions, where the black-dashed lines are the results from the one-skimmer image, and the red-solid lines are from the two-skimmers image. The projections in panel (d) have been normalized to the total count-rate, measured under the same experimental conditions.

B. Time-of-flight mass spectra

The direct effect of reducing background gas is the dramatic improvement of the signal-to-noise level. With the same experimental conditions as in Figure 2, the time-of-flight mass spectra of Ar^+ ions have also been recorded at hν = 17 eV in the one and two skimmer configurations and are displayed in Figure 3. Three isotopes of Ar with m/z = 36, 38, and 40 can be identified in the mass spectra, with ratios corresponding to their natural abundances, by far dominated by the ^{40}Ar isotope. Although the total ion counts have somewhat decreased (by a factor of about 2/3), the sensitivity of the TOF mass spectra was enhanced after installing the double skimmer geometry as it can be seen by the clear detection and separation of the m/z 38 isotope whose signal was buried in the noise in the single-skimmer geometry. In addition, the shape of the ^{40}Ar peak in the double-skimmer mass spectrum is more symmetrical than that in the one-skimmer mass spectrum in which the ^{40}Ar peak shows a long tail towards high mass due to the larger size of molecular beam.[33] This peak sharpening, and therefore enhanced resolution, in the double-skimmer geometry is clearly linked to the reduced size of the ionization region (visible in Fig. 2(b)). Indeed, this is a major issue in the case of the DELICIOUS III electrostatic structure for which unlike most TOF spectrometer, because of the presence of a VMI in the electron side, the gridless electrodes lead to a non-uniform electric extraction field. Therefore any reduction in the transverse size of the ionization region leads to a reduced sensitivity to the electric potential gradient induced by the hollow extractor electrode, and therefore to a sharpening of the mass spectrum peaks as well as a more uniform shape because of the strong reduction of the "long-TOF" tail.

Using the double-skimmer molecular beam, TOF mass spectra of Xe and its dimer Xe_2 were recorded at hν = 12.4 eV photon energy with a repeller voltage of 500 V and are presented in Figure 4. Nine isotopes of Xe have been identified and assigned in the TOF mass spectrum of Figure 4(a) with intensities matching their natural abundances. The peaks of the Xe_2 dimer have also been separated and can be easily assigned due to the present high mass resolution. From the peak of ^{132}Xe isotope in Figure 4(a), the mass resolution

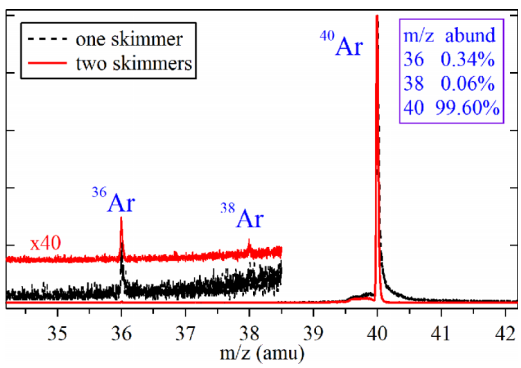

FIG. 3. TOF mass spectra of Ar isotopes recorded at hν = 17 eV with one skimmer (black-dashed line) and two skimmer (red-solid line) molecular beam configurations. The data with 40-times enlarged scale and the abundances of Ar isotopes have also been inserted.

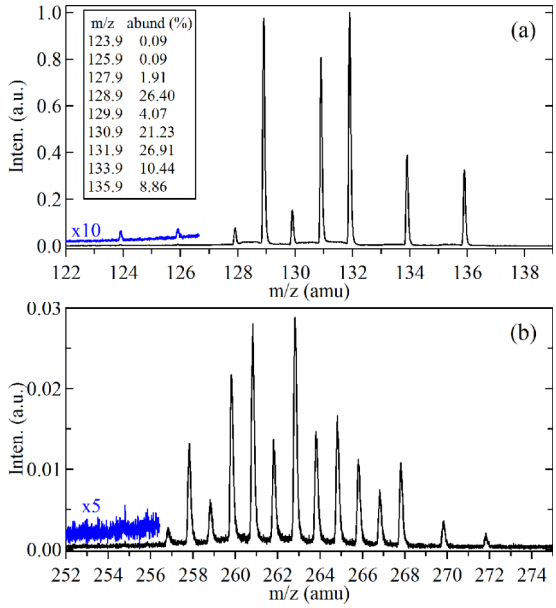

FIG. 4. TOF mass spectra of (a) Xe and (b) Xe_2 recorded at hν = 12.4 eV with a repeller voltage of 500 V.

is measured at close to M/ΔM = 1700 (FWHM), indicating that the present mass resolution has been increased more than a factor of 2 as compared to that of the single-skimmer molecular beam geometry[19] (this is clearly apparent from the comparison with Fig. 4 of Ref. 19). The mass resolution is high enough, typically 900 at 90% separation between adjacent peaks, to study state-to-state photochemistry corresponding to H-atom elimination of very large species such as polycyclic aromatic hydrocarbons (PAHs) or heavy-metal complexes by the PEPICO scheme.

C. Dissociative photoionization of O_2 at hν = 21.1 eV

Photoionization and dissociative photoionization studies of gas-phase molecules are one of the central subjects to be studied at the DESIRS beamline. As a prototype research system, dissociative photoionization of oxygen molecules involving the $O_2^+(B^2\sum_g^-)$ ionic state has been chosen and investigated with the DELICIOUS III spectrometer and the upgraded SAPHIRS double-skimmer configuration. The TOF mass spectrum was recorded at a fixed photon energy of hν = 21.1 eV and is displayed in Figure 5(a). Two peaks with m/z = 32 and 16 have been assigned as O_2^+ and O^+ ions, respectively. The O_2^+ ion peak from photoionization of nascent cold oxygen molecules exhibits a narrow and sharp shape. Two dissociation limits of O_2^+ ions, $O^+(^4S) + O(^3P)$ at 18.733 eV and $O^+(^4S) + O(^1D)$ at 20.700 eV, can be reached with the present photon energy.[36,37] The observed O^+ ions, which are formed by the dissociation of O_2^+, present a much larger width than the parent ions since a large kinetic energy is released in the dissociation.

The mass-selected electron and ion images corresponding to the O^+ fragment ions have also been recorded simultaneously and are presented in Figures 5(b) and 5(c). The polarization of synchrotron photons was set linear and its direction is horizontal, i.e., parallel to the propagation

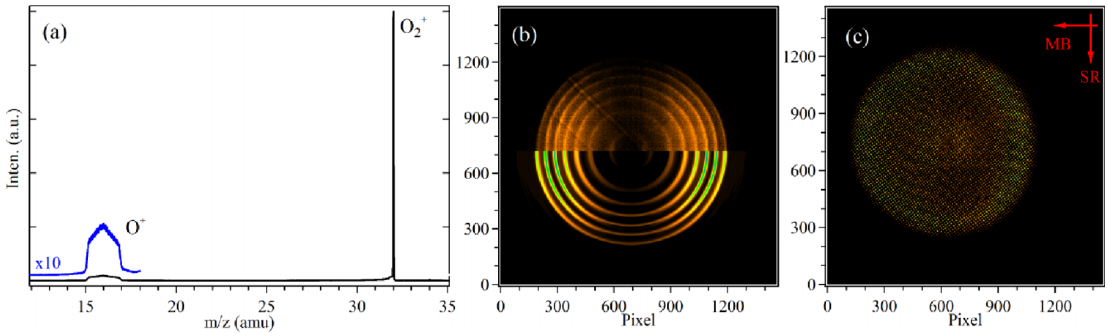

FIG. 5. (a) TOF mass spectrum and mass-selected (b) electron and (c) ion images corresponding to the O^+ fragment ion recorded at the fixed photon energy $h\nu = 21.1$ eV. The upper half of the electron image represents the raw data, and the lower one corresponds to the results from the pBasex Abel inversion algorithm.

direction of the molecular beam in the images. As the present experiment was mainly focusing on the $O_2^+(B^2\sum_g^-)$ electronic state, the extraction field of the DELICIOUS III spectrometer was set at 35 V cm^{-1} and only electrons with kinetic energies below 1.5 eV can be detected with no discrimination. In Figure 5(b), the upper half part of the electron image represents the raw data and the lower one corresponds to the results from the pBasex inversion algorithm.[34] Seven concentric rings can be clearly identified in the electron image. In Figure 5(c), the O^+ ion image takes the shape of a large circular pattern, corresponding to a large kinetic energy released (KER) in the dissociation.[38] In addition, due to the speed of the molecular beam, the ion image is exocentric with respect to the center of the ion PSD.

Correlating the electron and ion images in coincidence, the electron and ion kinetic energy correlation diagram was obtained and is displayed in Figure 6(a). Several intense points can be discerned in the correlation diagram and have been assigned as the $O_2^+(B^2\sum_g^-$, $v^+ = 0$-6) vibrational states[39] populated with the $h\nu = 21.1$ eV fixed energy photons, and which then dissociate into O^+ and O fragments. The correlation diagram can be divided into two parts based on the energy conservation in dissociation, the first part including seven spots with $iKE(O^+) > 0.7$ eV has a large intensity and can be assigned as the dissociation along the $O^+(^4S) + O(^3P)$ channel, while a weaker part with $iKE(O^+) < 0.2$ eV corresponds to the $O^+(^4S) + O(^1D)$ dissociation channel. Therefore, for $v^+ \geq 4$ there is competition between the two pathways, although from Fig. 6 it is clear that the $O^+(^4S) + O(^3P)$ path is the main fragmentation channel in the dissociation of $O_2^+(B^2\sum_g^-$, $v^+ = 0$-6) ions. The predissociation of the $O_2^+(B^2\sum_g^-)$ state to the lowest $O^+(^4S) + O(^3P)$ channel is accomplished mainly through the crossing with the $1^2\sum_g^+$, $f^4\prod_g$, and $d^4\sum_g^+$ states, while to the $O^+(^4S) + O(^1D)$ channel is via the $2^4\prod_g$ electronic state.[38]

The total center of mass KERs of the O^+ and O fragments dissociated from vibrational state-selected $O_2^+(B^2\sum_g^-$, $v^+ = 0$-6) ions can be directly obtained from the correlation diagram and are presented in Figures 6(b)-6(h). Comparing to previously measured data on N_2 in the single skimmer geometry, the present 3D ion kinetic energy resolution has been slightly improved (~15%) with the double-skimmer molecular beam configuration. The ray tracing simulations predict an average improvement of 25% on the resolution,

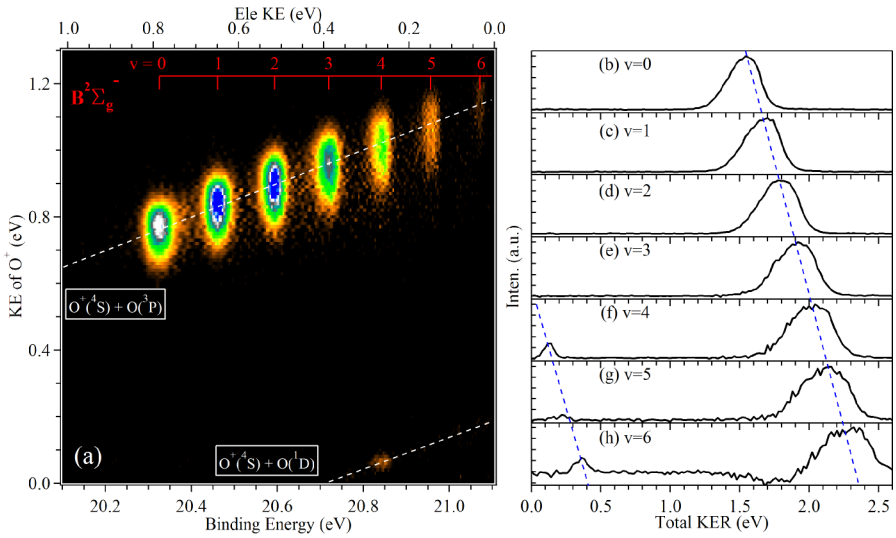

FIG. 6. (a) Electron and ion kinetic energy correlation diagram corresponding to the O^+ fragment ions recorded at $h\nu = 21.1$ eV; (b)-(h) total KERs in dissociation of vibrational-state-selected $O_2^+(B^2\sum_g^-$, $v^+ = 0$-6) ions. The two dissociation limits $O^+(^4S) + O(^3P)$ and $O^+(^4S) + O(^1D)$ are also marked with dashed lines in the figure.

which is slightly more optimistic than the experimental gain. The small discrepancy might be attributed to the lensing effect of the final mesh between the detector and the end of the ion tube, or to alignment/electrostatic issues. The latter has more impact on the ion side because the lens electrode used for the ion space focusing is located far from the interaction region.[19] The total KERs along both the $O^+(^4S) + O(^3P)$ and $O^+(^4S) + O(^1D)$ dissociation channels increase linearly with electron binding energy. The branching ratio of the $O^+(^4S) + O(^1D)$ minor channel in the total KER curves oscillates with electron binding energy. After appearing at the $v^+ = 4$ vibrational state, the $O^+(^4S) + O(^1D)$ channel almost vanishes at the $v^+ = 5$ state and then rises again at the $v^+ = 6$ state. The same phenomena have also been observed by the method of TPEPICO velocity imaging[18] with scanning of the synchrotron photon energy and the explanation of the oscillation has been introduced before.[38] The appearance of the $O^+(^4S) + O(^1D)$ channel at the $v^+ = 4$ site is attributed to the dissociation of the resonant $^2\sum_u^-(v^+ = 5)$ vibrational state.[40] The present results again demonstrate the multiplexed capabilities of the i^{2}PEPICO approach.

D. VMI electron energy resolution

Besides improving the vacuum capabilities of SAPHIRS, one of our main motivation for implementing a double-skimmer geometry was to improve the VMI electron KE energy resolution which at the best was $\Delta E/KE \sim 4\%$ on the edge of the VMI PSD with DELICIOUS III and a single-skimmer geometry.[19] This value was slightly worse than the one predicted by ray-tracing simulations with a 6 mm–long "cigar-shape" ionization volume and we attributed the discrepancy mainly to off-axis aberrations. The addition of the ion imaging has allowed us to measure directly the molecular beam size which, as mentioned above, is now estimated at 7 mm. The simulations now match the experimental energy curves for the single skimmer configuration, as seen in Figure 7.

Furthermore, a rather fortunate failure of our Roentdek ATR19 amplifier/discriminator multi-channel unit forced us to exchange it for another ATR19 unit, and we observed a marked improvement of the resolution already on the raw image, on which the final mesh in front of the electron PSD is for the first time clearly visible (see Fig. 7(a)). From the shadow of the mesh, we now estimate the spatial resolution of the detector at around 0.4 mm FWHM (170 μm RMS), which corresponds to a sizeable improvement from the 240 μm RMS measured with the faulty ATR19 board. We note that this value is well above the resolution of our in-house made ion PSD, which was estimated at below 50 μm.[41] The difference might be partly due to the delay time/mm conversion factors which are 2.2 times larger in the ion PSD (4.36 vs 1.97 ns/mm) leading to a better sampling by our 120 ps Time To Digital (TDC) converter.

More precisely the image and corresponding PES of N_2 photoionized at 19.5 eV show that we can reach on the edge of the detector a kinetic energy resolution of 2.8%, which to our knowledge represents the state of the art for a VMI combined with SR.[42,43] We attribute this spectacular improvement of the electron resolution to the better functioning of the 4 delay-line

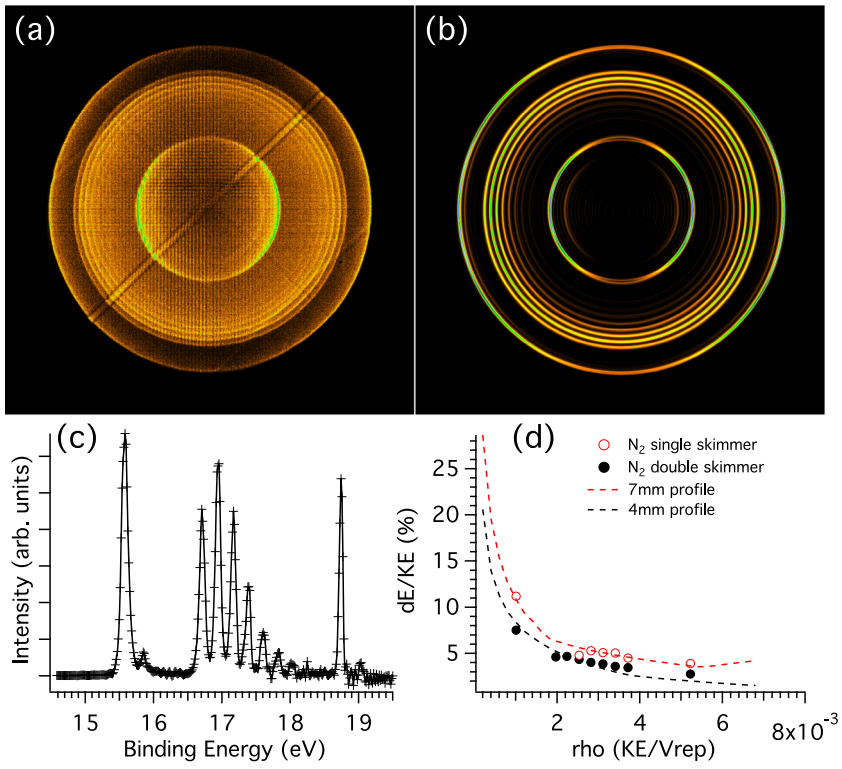

FIG. 7. Raw (a) and inverted (b) electron image of N_2 photoionized at 19.5 eV with a 750 V repeller voltage. (c) Corresponding PES showing an ultimate kinetic energy resolution of 2.8%. (d) Electron KE resolution curve obtained from the PES with a single (red open circles) and double (black open circles) skimmer configurations along with the predicted curves for a 7 mm (single skimmer) and 4 mm (double skimmer) reaction sizes.

signals since apparently in our former device the signal was misprocessed by a deficient electronic circuit. Of course, and as predicted by the simulations of the single and double skimmers shown in Fig. 7(d), the gain in resolution must also be attributed to the presence of the double skimmer because a similar spectrometer, DELICIOUS II, provided electron KE resolutions of the order of 5% at the detector's edge using the same in-house PSD with the <50 μm spatial resolution.[17] The ray-tracing simulations for the estimated 4 mm length of the doubly skimmed molecular beam show that the experimental performances are very close to the predicted values (see Fig. 7(d)). We note that the inversion errors due to the experimental noise that can degrade the observed resolution are not accounted for in the simulations and therefore could explain at least part of the small disagreement.

The 170 μm spatial resolution of the delay-line anode limits the energy resolution to dE/KE = 2.3% for the N_2^+ X state at 15.58 eV ($\rho = 5.2 \times 10^{-3}$ in Fig. 7(d)) which, as seen in Fig. 7(d), is perilously close to the experimentally measured 2.8%, and to the 2.0% predicted by the ray tracing simulations. Since the TDC step of 120 ps corresponds to 0.0610 mm, i.e., to dKE/KE = 0.17%, it means that further improvements are needed on the electronics chain (signal decoupling + amplification + discrimination) if one wants to descend below the present 2.8% value. Indeed, further resolution improvements are possible through the optimization of the extraction region geometry which would need the optimization of the electronic treatment. For instance, the two gridless electrodes could be shaped in a way as to minimize spherical aberrations of the electrostatic lens, and a third gridless electrode could be added, as already implemented in various designs, including commercially available VMIs, which claim down to 1% KE resolution in ion imaging experiments.[44,45] In addition, small stray electric fields are known to be present in our interaction region and might influence the final electron KE resolution by breaking the cylindrical symmetry of the resulting images, especially for slower electrons and low extraction fields. Most probably they are linked to the ceramic spacers between the electrodes and short-term plans to shield the ceramics with a metallic cover might further improve the shape of the electric field, which will improve the resolution, especially for TPES/TPEPICO experiments using very slow electrons.

IV. CONCLUSIONS

The SAPHIRS photoionization experimental end-station has been upgraded by installing a double-skimmer differential chamber to enhance the performances of the electron/ion coincidence end-station at the DESIRS VUV beamline of synchrotron SOLEIL, as well as the general vacuum capabilities of the whole set-up. Experimental results show that the size of the double-skimmed molecular beam in the ionization region has been reduced to nearly half that of a single-skimmer molecular beam geometry. Additionally, the mass resolution of the time-of-flight mass spectrum has been increased to M/ΔM ~ 1700, and the overall signal-to-noise level has been improved by reducing the amount of background gas.

As a representative application of the double-skimmed molecular beam, the dissociative photoionization of O_2 molecules at fixed photon energy, hν = 21.1 eV, has been investigated by using the i^{2}PEPICO spectrometer, DELICIOUS III. Vibrationally state-selected $O_2^+(B^2\sum_g^-, v^+ = 0\text{-}6)$ ions were prepared and then dissociated into O^+ and O fragments. The electron and ion kinetic energy correlation diagram of the O^+ fragment ions was recorded via the electron/ion coincidence scheme. The two dissociation channels of O_2^+ ions, $O^+(^4S) + O(^3P)$, and $O^+(^4S) + O(^1D)$, have been detected and identified in the correlation diagram and the total ion KER curves. The present detailed results demonstrate the multiplex capabilities of imaging electron/ion coincidences, even with a single energy VUV light source.

Besides we also show a spectacular enhancement of the electron energy resolution down to 2.8% due to the addition of the double skimmer and to a proper handling of the delay-line signals by the electronics. With this energy resolution associated with the demonstrated high mass resolution and ion imaging capabilities, and combined with the state-of-the-art VUV undulator-based beamline DESIRS, we believe that DELICIOUS III/SAPHIRS is a state-of-the-art efficient and versatile set-up for the study of valence-shell molecular VUV photodynamics.

ACKNOWLEDGMENTS

We acknowledge the financial support from the French Agence Nationale de la Recherche (ANR) under Grant No. ANR-12-BS08-0020-02 (project SYNCHROKIN). We would like to thank the SOLEIL staff for smoothly running the synchrotron facility and providing beamtime under Proposal Nos. 20140090 and 99150038. We are also grateful to D. Dowek for lending us her Roentdek ATR-19 unit.

[1]D. W. Turner, C. Baker, A. D. Baker, and C. R. Brundle, *Molecular Photoelectron Spectroscopy: A Handbook of He 584 Å Spectra* (Wiley, London, 1970).
[2]J. H. D. Eland, *Photoelectron Spectroscopy: An Introduction to Ultraviolet Photoelectron Spectroscopy in the Gas Phase* (Butterworths, London, 1984).
[3]I. Powis, T. Baer, and C. Y. Ng, *High Resolution Laser Photoionization and Photoelectron Studies* (Wiley, Chichester, 1995).
[4]C. Y. Ng, Annu. Rev. Phys. Chem. **53**, 101 (2002).
[5]U. Becker and D. A. Shirley, *VUV and Soft X-Ray Photoionization* (Plenum, New York, 1996).
[6]S. S. Wang, R. H. Kong, X. B. Shan, Y. W. Zhang, L. S. Sheng, Z. Y. Wang, L. Q. Hao, and S. K. Zhou, J. Synchrotron Radiat. **13**, 415 (2006).
[7]M. Johnson, A. Bodi, L. Schulz, and T. Gerber, Nucl. Instrum. Methods Phys. Res., Sect. A **610**(2), 597 (2009).
[8]L. Nahon, N. de Oliveira, G. A. Garcia, J. F. Gil, B. Pilette, O. Marcouille, B. Lagarde, and F. Polack, J. Synchrotron Radiat. **19**, 508 (2012).
[9]P. A. Heimann, M. Koike, C. W. Hsu, D. Blank, X. M. Yang, A. G. Suits, Y. T. Lee, M. Evans, C. Y. Ng, C. Flaim, and H. A. Padmore, Rev. Sci. Instrum. **68**(5), 1945 (1997).
[10]Y. Li and F. Qi, Acc. Chem. Res. **43**, 68 (2009).
[11]B. Sztaray, A. Bodi, and T. Baer, J. Mass Spectrom. **45**(11), 1233 (2010).
[12]A. Bodi, P. Hemberger, D. L. Osborn, and B. Sztaray, J. Phys. Chem. Lett. **4**(17), 2948 (2013).
[13]P. O'Keeffe, P. Bolognesi, M. Coreno, A. Moise, R. Richter, G. Cautero, L. Stebel, R. Sergo, L. Pravica, Y. Ovcharenko, and L. Avaldi, Rev. Sci. Instrum. **82**(3), 033109 (2011).
[14]T. Baer, *Gas Phase Ion Chemistry* (Academic, New York, 1979).
[15]T. Baer and W. L. Hase, *Unimolecular Reaction Dynamics: Theory and Experiments* (Oxford University Press, 1996).

[16]A. Bodi, P. Hemberger, T. Gerber, and B. Sztaray, Rev. Sci. Instrum. **83**(8), 083105 (2012).
[17]G. A. Garcia, H. Soldi-Lose, and L. Nahon, Rev. Sci. Instrum. **80**(2), 023102 (2009).
[18]X. F. Tang, X. G. Zhou, M. L. Niu, S. L. Liu, J. D. Sun, X. B. Shan, F. Y. Liu, and L. S. Sheng, Rev. Sci. Instrum. **80**(11), 113101 (2009).
[19]G. A. Garcia, B. K. C. de Miranda, M. Tia, S. Daly, and L. Nahon, Rev. Sci. Instrum. **84**(5), 053112 (2013).
[20]A. Eppink and D. H. Parker, Rev. Sci. Instrum. **68**(9), 3477 (1997).
[21]W. C. Wiley and I. H. McLaren, Rev. Sci. Instrum. **26**(12), 1150 (1955).
[22]M. Richard-Viard, A. Delboulbe, and M. Vervloet, Chem. Phys. **209**(2-3), 159 (1996).
[23]See http://www.synchrotron-soleil.fr/Recherche/Bibliotheque/DocumentationScientifique/DESIRS for a general description of the DESIRS beamline.
[24]M. Briant, L. Poisson, M. Hochlaf, P. de Pujo, M.-A. Gaveau, and B. Soep, Phys. Rev. Lett. **109**(19), 193401 (2012).
[25]H. Dossmann, G. A. Garcia, L. Nahon, B. K. C. de Miranda, and C. Alcaraz, J. Chem. Phys. **136**(20), 204304 (2012).
[26]X. F. Tang, G. A. Garcia, and L. Nahon, J. Phys. Chem. A **119**, 5942 (2015).
[27]X. F. Tang, G. A. Garcia, and L. Nahon, Phys. Chem. Chem. Phys. **17**, 16858 (2015).
[28]D. M. P. Holland, E. A. Seddon, S. Daly, C. Alcaraz, C. Romanzin, L. Nahon, and G. A. Garcia, J. Phys. B **46**(9), 095102 (2013).
[29]I. Powis, S. Daly, M. Tia, B. C. de Miranda, G. A. Garcia, and L. Nahon, Phys. Chem. Chem. Phys. **16**(2), 467 (2014).
[30]M. Tia, B. C. de Miranda, S. Daly, F. Gaie-Levrel, G. A. Garcia, I. Powis, and L. Nahon, J. Phys. Chem. Lett. **4**(16), 2698 (2013).
[31]G. A. Garcia, H. Dossmann, L. Nahon, S. Daly, and I. Powis, Phys. Chem. Chem. Phys. **16**(30), 16214 (2014).
[32]F. Gaie-Levrel, G. A. Garcia, M. Schwell, and L. Nahon, Phys. Chem. Chem. Phys. **13**(15), 7024 (2011).
[33]G. A. Garcia, X. F. Tang, J. F. Gil, L. Nahon, M. Ward, S. Batut, C. Fittschen, C. A. Taatjes, D. L. Osborn, and J. C. Loison, J. Chem. Phys. **142**(16), 164201 (2015).
[34]G. A. Garcia, L. Nahon, and I. Powis, Rev. Sci. Instrum. **75**(11), 4989 (2004).
[35]R. A. Livingstone, J. O. F. Thompson, M. Iljina, R. J. Donaldson, B. J. Sussman, M. J. Paterson, and D. Townsend, J. Chem. Phys. **137**(18), 184304 (2012).
[36]M. Richardviard, O. Dutuit, M. Lavollee, T. Govers, P. M. Guyon, and J. Durup, J. Chem. Phys. **82**(9), 4054 (1985).
[37]A. Lafosse, J. C. Brenot, A. V. Golovin, P. M. Guyon, K. Hoejrup, J. C. Houver, M. Lebech, and D. Dowek, J. Chem. Phys. **114**(15), 6605 (2001).
[38]X. F. Tang, X. G. Zhou, M. L. Niu, S. L. Liu, and L. S. Sheng, J. Phys. Chem. A **115**(24), 6339 (2011).
[39]M. Evans, S. Stimson, C. Y. Ng, C. W. Hsu, and G. K. Jarvis, J. Chem. Phys. **110**(1), 315 (1999).
[40]X. F. Tang, X. G. Zhou, M. M. Wu, Y. Cai, S. L. Liu, and L. S. Sheng, J. Phys. Chem. A **116**(38), 9459 (2012).
[41]D. Ceolin, G. Chaplier, M. Lemonnier, G. A. Garcia, C. Miron, L. Nahon, M. Simon, N. Leclercq, and P. Morin, Rev. Sci. Instrum. **76**(4), 043302 (2005).
[42]P. O'Keeffe, V. Feyer, P. Bolognesi, M. Coreno, C. Callegari, G. Cautero, A. Moise, K. C. Prince, R. Richter, R. Sergo, M. Alagia, M. de Simone, A. Kivimaki, M. Devetta, T. Mazza, P. Piseri, V. Lyamayev, R. Katzy, F. Stienkemeier, Y. Ovcharenko, T. Moller, and L. Avaldi, Nucl. Instrum. Methods Phys. Res., Sect. B **284**, 69 (2012).
[43]F. J. Furch, S. Birkner, J. H. Jungmann, F. Kelkensberg, C. P. Schulz, A. Rouzee, and M. J. J. Vrakking, J. Chem. Phys. **139**(12), 124309 (2013).
[44]See http://www.velocitas-vmi.com/ for general information on their commercial VMI spectrometers.
[45]D. Niu, Y. Ogi, Y.-I. Suzuki, and T. Suzuki, J. Phys. Chem. A **115**(11), 2096 (2011).